JCI insight

Loss of habenular *Prkar2a* reduces hedonic eating and increases exercise motivation

Edra London, Jason C. Wester, Michelle S. Bloyd, Shelby Bettencourt, Chris J. McBain, Constantine A. Stratakis

JCI Insight. 2020. https://doi.org/10.1172/jci.insight.141670.

Research In-Press Preview **Metabolism** **Neuroscience**

The habenula (Hb) is a bilateral, evolutionarily conserved epithalamic structure connecting forebrain and midbrain structures that has gained attention for its roles in depression,(1) addiction,(2-5) rewards processing,(6) and motivation (7,8). Of its two major subdivisions, the medial (MHb) and lateral Hb (LHb), MHb circuitry and function is poorly understood relative to LHb (9). *Prkar2a* codes for cAMP-dependent protein kinase (PKA) regulatory subunit IIα (RIIα), a component of the PKA holoenzyme at the center of one of the major cell-signaling pathways conserved across systems and species. Type 2 regulatory subunits (RIIα, RIIβ) determine the subcellular localization of PKA, and unlike other PKA subunits, *Prkar2a* has minimal brain expression except in the MHb (10). We previously showed that RIIα knockout (RIIαKO) mice resist diet-induced obesity (DIO) (11). In the present study, we report that RIIαKO mice have decreased consumption of palatable, “rewarding” foods and increased motivation for voluntary exercise. *Prkar2a* deficiency led to decreased habenular PKA enzymatic activity and impaired dendritic localization of PKA catalytic subunits in MHb neurons. Re-expression of *Prkar2a* in the Hb rescued this phenotype confirming differential roles for *Prkar2a* in regulating the drives for palatable foods and voluntary exercise. Our findings show that in the MHb decreased PKA signaling and dendritic PKA activity decrease motivation for food rewards while enhancing the motivation for exercise, a desirable combination of […]

Loss of habenular *Prkar2a* reduces hedonic eating and increases exercise motivation

Edra London[1], Jason C. Wester[2], Michelle Bloyd[1], Shelby Bettencourt[1], Chris J. McBain[2], Constantine A. Stratakis[1]

[1]Section on Endocrinology and Genetics, Eunice Kennedy Shriver National Institute for Child Health and Human Development, National Institutes of Health, Bethesda, MD 20892; [2] Section on Cellular and Synaptic Physiology, Eunice Kennedy Shriver National Institute for Child Health and Human Development, National Institutes of Health, Bethesda, MD 20892

Corresponding author: Edra London
10 Center Drive, Bldg 10/CRC, room #1-3216E
Bethesda, MD 20892
edra.london@nih.gov
+1 (301) 451-8250

Abstract

The habenula (Hb) is a bilateral, evolutionarily conserved epithalamic structure connecting forebrain and midbrain structures that has gained attention for its roles in depression,[1] addiction,[2-5] rewards processing,[6] and motivation.[7,8] Of its two major subdivisions, the medial (MHb) and lateral Hb (LHb), MHb circuitry and function are poorly understood relative to LHb.[9] *Prkar2a* codes for cAMP-dependent protein kinase (PKA) regulatory subunit IIα (RIIα), a component of the PKA holoenzyme at the center of one of the major cell-signaling pathways conserved across systems and species. Type 2 regulatory subunits (RIIα, RIIβ) determine the subcellular localization of PKA, and unlike other PKA subunits, *Prkar2a* has minimal brain expression except in the MHb.[10] We previously showed that RIIα knockout (RIIαKO) mice resist diet-induced obesity (DIO).[11] In the present study, we report that RIIαKO mice have decreased consumption of palatable, "rewarding" foods and increased motivation for voluntary exercise. *Prkar2a* deficiency led to decreased habenular PKA enzymatic activity and impaired dendritic localization of PKA catalytic subunits in MHb neurons. Re-expression of *Prkar2a* in the Hb rescued this phenotype confirming differential roles for *Prkar2a* in regulating the drives for palatable foods and voluntary exercise. Our findings show that in the MHb decreased PKA signaling and dendritic PKA activity decrease motivation for palatable foods, while enhancing the motivation for exercise, a desirable combination of behaviors.

Introduction

In the face of the global obesity epidemic, it remains unclear what makes some individuals more susceptible to obesity than others. Years of cumulative data show that the seemingly simple idea of balancing caloric intake with energy expenditure is complex and influenced by many opposing drives that are exacerbated by overscheduled sedentary lifestyles, changes in the food supply, and genetics.[12] As a major player in the regulation of the midbrain monoaminergic system,[6] the Hb is a central structure that integrates rewards with cognition and emotion.[13] While these Hb functions have been investigated in the context of substance abuse, a role for the Hb in obesity and susceptibility to the energy imbalance that drives preventable metabolic dysregulation is less clear.

To date, MHb research has primarily centered around addiction and mood-related disorders.[2] The MHb integrates the dysregulated rewards signaling that underlies the imbalance between reward seeking and avoidance behaviors in depression and substance abuse,[2,14] and it has been suggested that this circuitry may be important to obesity, it has not been systematically investigated. While LHb connectivity and function has been more extensively studied[15] it is increasingly evident that there may be complementary or synergistic roles for the MHb and LHb in regulating stress response, nociception, rewards, locomotor activity and food intake. In the regulation of hedonic eating, the LHb mediates inhibition of palatable food intake through glutamatergic neurons that project from the lateral hypothalamus.[16] Crosstalk between the MHb and LHb is unidirectional from MHb to LHb,[17] and while the interpeduncular nucleus (IPN) is a primary output target of both the LHb and MHb, each innervates distinct IPN structures.[18,19]

The MHb is subdivided into dorsal (dMHb) and ventral MHb subnuclei (vMHb), which can be identified by high expression of substance P or acetylcholine, respectively.[20-22] Developmental elimination of dMHb neurons via deletion of the transcription factor *Pou4f1* blunted sucrose preference,[8] but a deeper understanding of which cell populations in the MHb can regulate food rewards or signal satiety is lacking. We show here that *Prkar2a,* which codes for the cAMP-dependent protein kinase (PKA) regulatory subunit IIα (RIIα)**,** is highly expressed in the MHb in a region that overlaps the dMHb and vMHb subnuclei and is therefore present in both acetylcholine- and substance P-expressing cells.

The few animal studies investigating PKA signaling in the MHb have demonstrated neuroendocrine functions via both pre- and post-synaptic modulation of PKA activity.[23-25] In MHb axons, selective inhibition of PKA reversed the induction of glutamate release by atrial natriuretic peptide that plays a role in stress-induced analgesia.[25] Additionally, the modulation of local cAMP levels in MHb NAChRs regulates nicotine intake through the diabetes-associated gene, TCF7LR.[4] These studies provide clear and divergent evidence for regulatory roles for PKA in the Hb, but the breadth of knowledge about specific roles of PKA activity or its inhibition in the MHb is incomplete. In mice, deletion of *Prkar2a* led to a DIO-resistant phenotype and improved glucose tolerance after chronic HFD-feeding.[11] There was no detectable metabolic phenotype under normal feeding conditions.[11,26] The observed DIO-resistance, that was more prominent in female mice, could not be fully explained by altered metabolic rate that was only modestly increased after high-fat diet (HFD) exposure,[11] but instead appeared to be the result of decreased HFD intake. Here, we explore how *Prkar2a* might regulate behaviors related to food intake, the motivation for natural rewards, and energy expenditure, and how PKA signaling in the MHb might be altered by the deletion of *Prkar2a*.

Results

Prkar2a expression is localized to both substance P- and acetylcholine-expressing cells in the MHb

Combinations of two PKA catalytic (Cα, Cβ, Cγ) and two PKA regulatory (RIα, RIβ, RIIα, RIIβ) subunits form the PKA holoenzyme; isoform composition of the tetrameric enzyme is tissue-specific and affects cAMP binding affinity and cellular localization. All subunits except for RIIα have high brain expression, yet expression for each appears to be specific,[10] and largely non-redundant. At both RNA and protein levels, RIIα was expressed in both the dMHb and vMHb and around the junction of the two subnuclei (Fig 1A). The virtual absence of *Prkar2a* in other brain regions is evident from whole brain view, 3-D *in situ* hybridization (ISH) data (Fig 1B, Allen Brain Institutes). Because the habenular structure changes morphologically anterior to posterior, we mapped the expression of *Prkar2a* throughout the Hb from bregma -1.0 mm to -2.0mm and found that *Prkar2a* expression peaked between bregma-1.3– -1.7mm (Suppl Fig 1A). These mapping studies also show that *Prkar2a* expression patterns throughout the dMHb and vMHb vary from anterior to posterior points in the MHb. We used ISH with probes for *Syn-1* and *Gfap* to establish *Prkar2a* expression in both neuronal and glial cells of the MHb (Suppl Fig 1B). Both MHb and LHb neurons use glutamate as their primary neurotransmitter.[27,28]

We initially confirmed that *Prkar2a* expression was limited to glutamatergic neurons and not expressed in a subset of GABAergic cells in WT mice by ISH using probes for *Slc17a7* and *Gad1* (Suppl Fig 1C). In line with our expression studies, *Prkar2a* was the only PKA regulatory subunit identified as a highly and differentially expressed gene among the identified cell subsets within the MHb via single-cell

transcriptome analysis of mouse.[29] High relative expression of *Slc17a6* and *Slc17a7*, that code for vesicular glutamate transporters 1 and 2, and *Tac2* (coding for tachykinin precursor 2) were a common feature among five distinct neuronal cell populations identified in the MHb.[29] To characterize the subsets of *Prkar2a*-expressing glutamatergic cells, we performed ISH with probes for *Chat*, *Tac1*, *Tac2*, and *Tac1r*. *Prkar2a* was colocalized with choline acetyltransferase (*Chat*) primarily in vMHb (Figs 1C–D) and with tachykinin precursor 1 (*Tac1*) in the dMHb and to a lesser extent in the vMHb (Fig 1D). *Tac2* was distributed throughout the dMHb and vMHb and was expressed in 65.02 ± 2.20 % of *Prkar2a*-expressing cells (Figs 1E, G). Similarly, *Tac1* was expressed in 46.11 ± 7.26 % *Prkar2a*-expressing cells in the MHb, where these genes are highly and specifically expressed (Figs 1D-E, 1G). *Tac1r* was expressed in 39.99 ± 7.01 % in *Prkar2a*-expressing cells (for which substance P is the substrate) (Fig 1F-G), and *Chat* was expressed in 15.10 ± 1.45 % of the *Prkar2a*-expressing cells (Figs 1C-D, 1G). The colocalization studies showed that *Prkar2a* is expressed in a heterogenous population of MHb cells and is expressed in both substance P- and acetylcholine-producing neurons.

Habenular PKA enzymatic activity is decreased in RIIαKO mice

In the Hb of RIIαKO mice, cAMP-stimulated PKA enzymatic activity was significantly decreased and basal activity tended to be blunted (Fig 2A, left). However, PKA enzymatic activity was unchanged in pre-frontal cortex and striatum, two regions that provide direct input to the Hb (Fig 2A). Thus, disrupted cAMP signaling in the MHb is due to cell-autonomous *Prkar2a* deficiency. Further, the impact on cAMP-stimulated PKA activity suggests a blunted response to upstream signaling events in response to stimuli and not just a generalized decrease in activation under basal conditions.

Because cells in the vMHb release acetylcholine onto the interpeduncular nucleus (IPN), the primary efferent of the MHb, we measured acetylcholine levels in the IPN. The habenula highly expresses NAchR, subtypes α3, β3 and β4 and therefore, habenular acetylcholine concentrations were also measured. Acetylcholine concentrations were significantly lower in both the Hb and IPN of RIIαKO compared to WT mice (Fig 2B). Additionally, we found comparable levels of glutamate in Hb between genotypes and decreased glutamate concentrations in the IPN in RIIαKO mice (Fig 2C). To investigate alterations in the PKA subunit expression in the Hb, we quantified the mRNA and protein levels of the PKA subunits known to compensate for perturbations in the PKA system. mRNA levels of *Prkar1a* and *Prkaca* did not differ in RIIαKO Hb compared to WT mice, but RIα protein tended to be lower and Cα was significantly reduced in RIIαKO Hb lysates (Figs 2D–E). Total PKA catalytic subunit (α, β, and γ) protein levels were also lower in Hb of RIIαKO mice (Fig 2E). This is not unexpected as PKA is typically not regulated at the transcriptional level, but is instead regulated via post-translational changes in the stability of the PKA holoenzyme or free catalytic subunit.[30]

Localization of PKA catalytic subunits to MHb dendrites is disrupted in RIIαKO mice

Cellular localization of the PKA catalytic subunits and RIIα was investigated in the MHb at the point where dMHb and vMHb meet in the center of the structure. Altered subcellular localization of PKA subunits can affect neuronal signaling and impact cellular function and phenotypic characteristics.[31] PKA catalytic subunits localized to both the cytoplasm and the nucleus within the cell body, and to the dendrites in the MHb of WT mice (Fig 2F, left panel). In RIIαKO mice, however, localization of PKA catalytic subunits in dendrites was severely impaired and total catalytic subunit expression appeared to be decreased, a feature that was confirmed quantitatively by western blot (Fig 2F, right panel; Fig 2E). In

WT mice, PKA RIIα was localized to the cytoplasm as well as to dendrites in MHb neurons, that was absent in RIIαKO mice (Fig 2G). MHb excitatory inputs come through the stria medullaris from the septum, nucleus accumbens (NAc) and the cholinergic broca diagonal band,[13,32,33] and high expression of GABA-B receptors in the MHb[34,35] suggests strong inhibitory inputs. The diverse connectivity of the MHb demonstrates a clear linkage to rewards circuitry involving both inhibitory and excitatory inputs that could be disrupted by impaired post-synaptic signaling due to PKA deficiency in the MHb.

RIIαKO mice have decreased intake of palatable food when provided chronic ad-libitum access

To determine whether RIIαKO mice consume less palatable HFD when given free access, we provided young adult male and female RIIαKO and WT littermate mice with *ad libitum* HFD for 3 weeks. Female RIIαKO mice consumed less energy than their WT littermates (p=0.0091, two-way ANOVA), a phenomenon not observed in male mice (Fig 3A). Differences between genotypes were greater before adjusting for body weight (data not shown). Binge-eating affects both sexes, but occurs more often in women,[36] a sex difference that has been replicated in rodent models.[37] Studies with dopamine (DA) antagonists have demonstrated that DA is important for the learned responses to food that relate directly to food reward reinforcement. [38,39] Removal of HFD after chronic exposure drives dysregulation of DA signaling in female, but not male mice. Interestingly, when exposed to HFD for longer periods of time, a pattern of significantly reduced intake emerged in male RIIαKO mice (data not shown). Cumulative energy intake for the 3wk study was significantly higher in female WT compared to KO mice (WT: 13.50 ± 0.51 kcal/g BW and KO: 11.76 ± 0.33 kcal/g BW) and did not differ between males (data not shown). Female RIIAKO mice tended to gain less weight during HFD-feeding (*P* = 0.059) (Fig 3B), and metabolic efficiency did not differ significantly from WT littermates (Fig 3C) consistent with our previous

indirect calorimetry studies that showed only small difference in resting VO^2 during HFD- but not CD-feeding.[11]

Palatable foods are naturally rewarding and their consumption leads to the acute striatal DA release.[40] While striatal PKA enzymatic activity wasn't altered in RIIαKO mice on a normal chow diet *in vitro*, HFD increases striatal PKA signaling and alters phosphorylation of DA- and cAMP-regulated phosphoprotein-32 (DARPP-32) in mice.[41] DARPP-32 is a key integrator of DA and glutamate signaling in the basal ganglia that is highly expressed in striatal spiny neurons and can act either as an inhibitor of protein phosphatase 1 or PKA via T^{34} or T^{75} phosphorylation, respectively.[42] Based on this and habenular complex connectivity in which the MHb is a central mediator of DA signaling between NAc and VTA,[13] we investigated striatal phosphorylation of DARPP-32 . We found significant alterations in DARPP-32 phosphorylation after chronic HFD- but not CD-feeding in KO compared to WT mice. Phosphorylation of DARPP-32 at Thr^{34} was decreased in mutant mice after HFD but not CD-feeding compared to WT littermates (Fig 3D; top: CD, bottom: HFD). Phosphorylation of DARPP-32 at Thr^{75} was unchanged in RIIαKO mice irrespective of diet (Fig 3D). Striatal sections from WT and RIIαKO mice stained for DARPP-32 did not appear to have different cellular distribution of DARPP-32 (Fig 3E). Decreased striatal DARPP-32 has been reported in the ΔFosB mouse, a model of increased reward sensitivity characterized by decreased HFD intake and lower levels of striatal pCREB.[43] Our results suggest that blunted striatal DARPP-32 T^{34} phosphorylation is associated with decreased intake of HFD in RIIαKO mice. Rodent studies have shown that chronic HFD causes changes in the DA signaling system, including lower basal DA levels in the NAc.[40,44] Furthermore, acute or chronic treatment with the selective serotonin reuptake inhibitor, fluoxetine led to increased phosphorylation of DARPP-32 at Thr^{34} and decreased phosphorylation at Thr^{75} in striatum.[45] Here we show differences in striatal DARPP-32 phosphorylation

in RIIαKO mice after 3wk HFD feeding and decreased intake among mutant females and males (over a longer period of HFD exposure).

Fasted RIIAKO mice have decreased drive for food reward

RIIαKO and WT littermates trained to perform an operant lever press task on a fixed ratio schedule of food pellet delivery were then subjected to a progressive ratio operant task in both the fed and fasted states. There were no differences in learning the operant task as assessed by percent correct and incorrect lever presses and in achieving the goal of earning 50 food pellets with at least 80% correct lever presses (data not shown). Additionally, the amount of time spent engaged in the operant task and the drive to work for food reward assessed (i.e., breakpoint) in non-fasted mice did not differ between genotypes (Figs 4A-C). After a 14h overnight fast, RIIαKO mice spent less time engaged in the progressive ratio task (Fig 4A), had a lower breakpoint and earned fewer food reward pellets than their WT littermates (Figs 4B-C).

RIIAKO mice drink less sucrose solution and have blunted sucrose preference

To further evaluate the role of *Prkar2a* in hedonic drive for natural rewards, we performed sucrose preference tests in male and female mice using 10% (wt/vol) sucrose solution and a standard two-bottle paradigm. Sucrose preference is a well-established test for anhedonia, defined as the lack of ability to experience pleasure from rewarding or enjoyable activities.[46] When given 24h access to both 10% sucrose and water for 3 consecutive days per week over a 2-week period, multiple comparisons

revealed similar sucrose intakes between WT and RIIAKO mice on day 1, but RIIAKO mice had lower intake levels than WT mice on subsequent days (Fig 4D). There was a significant genotype effect on sucrose intake for female and male mice ($P = 0.0095$, $P = 0.0053$, two-way ANOVA). Similarly, after the initial 24h period, sucrose preference was significantly decreased in male RIIAKO mice ($P = 0.0073$), highlighting a sex difference in the *Prkar2a*-mediated regulation of sucrose reward (Fig 4E).

Despite the lack of differences in energy intake from chow between genotypes (data not shown), male RIIαKO mice had decreased total energy intake due to differences in sucrose consumption and gained less weight than WT littermates during the 2wk experiment (Figs 4F-G). There were no differences in cumulative total energy intake or weight gain after sucrose access in female mice (Figs 4F-G).

Circuits between the lateral hypothalamus and the VTA, an indirect target of the MHb, play a role in sucrose seeking and reward encoding,[47] and tachykinins (derived from the MHb) are involved in umami and perhaps other taste modalities.[48] VTA glutamate neurons have also been associated with positive reinforcement during reward-based operant tasks mediated by their release of GABA.[49] Thus, disruption of these signals through decreased MHb signaling to the VTA via the IPN may act to impair reward processing and reinforcement.

RIIAKO mice have increased drive for voluntary running

Motivation for exercise can play an important role in energy homeostasis and this drive is regulated by shared circuitry that regulates other natural rewards yet has distinctions from those mediating food reward (i.e., taste vs locomotor activity). The Hb plays a role in regulating the temporal pattern of

237 locomotor activity throughout the night.[50] Moreover, both developmental ablation of dMHb neurons, or
238 maturation defects in the MHb severely impair voluntary wheel running behavior in mice.[7,8] Thus, we
239 investigated voluntary exercise performance of RIIαKO mice. When provided with home cage running
240 wheels, RIIαKO mice ran 2-3 times the distance than that of their WT littermates (Fig 5A-B). *Prkar2a*
241 heterozygosity rescued the high running phenotype of RIIαKO mice to levels of WT mice. These data
242 suggest that even partial restoration of RIIα-mediated PKA activity and holoenzyme localization suffices
243 to reverse the change in PKA signaling responsible for the observed motivation for running. Total wheel
244 turns for the 2-week running experiment was significantly lower for both WT and RIIα+/- mice compared
245 to RIIαKO mice for both sexes (Fig 5A-B). The timing of running activity across light:dark cycles and
246 within the active dark cycle was as expected with spikes of activity in the early dark period and tapered
247 activity in the later part of the dark cycle and did not differ among genotypes. We previously showed
248 that normal home cage locomotor activity was not different between WT and RIIαKO mice of either
249 sex.[11] Denial of the expected access to running wheels was identified as activating striatum, lateral
250 hypothalamus and frontal cortex in mice selectively bred for running, suggesting that omission of
251 reward led to anxiety or stress.[51]

252

253 Given the increased motivation for running in RIIαKO mice, we hypothesized that mutant mice
254 accustomed to daily wheel running might experience stress that could be detected by Hb activation in
255 the absence of this natural reward. The MHb was identified as one of six limbic regions that are
256 susceptible to stress-induced c-Fos expression[52] and c-Fos was identified in MHb and LHb in response to
257 restraint stress and forced swim test.[53] Therefore, we decided to assess both c-Fos and c-Jun expression
258 in response to being blocked from the expected running wheel access. In RIIαKO mice, blocking access to
259 running wheels prior to onset of the dark cycle resulted in increased c-Fos and c-Jun expression in the
260 MHb (Figs 5D-E). Induction of c-Fos and c-Jun was not observed in the MHb of WT mice that were

blocked from running. Regardless of genotype, no immediate early gene (IEG) induction in the Hb was observed in mice that had continued access to running wheels (Fig 5D, right panels), suggesting that hyperactivation of the MHb may be associated with stress or anxiety related to withholding the pleasurable experience of running. Additionally, when similar studies were conducted after mice were habituated to sucrose access, no IEG induction was observed in WT or KO mice under either reward or blocked reward conditions (data not shown).

rAAV-mediated habenular Prkar2a re-expression rescues sucrose preference and running phenotypes

We hypothesized that the behavioral phenotypes observed were driven specifically by *Prkar2a* deletion in the Hb. We delivered a recombinant adeno-associated viral (rAAV) vector with a construct containing *Prkar2a* and GFP via bilateral stereotaxic injections to young adult WT and RIIαKO mice (both sexes) (Fig 6A). Pilot injections first with retrobeads and then with a GFP-containing rAAV were used to confirm injection coordinates. Post-experimental injection accuracy was confirmed by immunofluorescence for each mouse (Suppl Fig 2; Fig 6B is a representative image of the expected re-expression of PKA RIIα). RIIαKO mice with off-target injections were classified by lack of immunofluorescent signal for RIIα and GFP in the MHb and subsequently excluded from the data analysis. Two to 3-weeks after a surgery, a period that was sufficient for recovery, and to ensure adequate RIIα protein expression, sucrose preference tests were performed followed by a 2-week washout period prior to initiating 2-week running wheel experiments. Re-expression of *Prkar2a* in the MHb rescued the sucrose intake and preference phenotype of RIIαKO mice (Fig 6C) as well as the increased voluntary running phenotype (Fig 6D). There were no differences between mean sucrose intake or preference levels or of total wheel

turns in the rAAV-injected WT or rAAV-injected RIIαKO mice, confirming that habenular *Prkar2a* inversely regulates voluntary exercise and sweet reward responses.

Discussion

Across species, a positive response to natural rewards is an innate survival mechanism that is driven by the cognitive processing of pleasure experienced from activities like eating, running (as prey or predator), or sex. While being able to experience the rewarding aspects of food is evolutionarily vital, overriding satiety signals in favor of the overconsumption of high-fat and sweet foods can lead to obesity, metabolic dysregulation, and other related comorbidities. Achieving weight loss and maintaining energy balance by moderating food intake and increasing physical activity underlies the battle against dietary obesity and weight gain. The habenula is central to reward and aversion systems which are both necessary for maintaining balance in processing rewards stimuli. The LHb is critical in transmitting negative-reward signals and a rewarding stimuli causes decreased LHb activity in concert with increased DA activity, while the reverse is true of punishing stimuli.[6,54] While, the habenula has been hypothesized to serve as nexus of the complex reward circuitry with a key role in maintaining the balance between reward-seeking and avoidance behaviors,[2] much less is known about the roles for the MHb in these processes.

Here we identify an unexpected role for PKA RIIα in the MHb in the simultaneous positive regulation of food rewards and negative effect on the drive to exercise, behaviors that were both reversed with RIIα

deficiency. The diminishment of both drives is characteristic of the anhedonia observed in major depressive disorder (MDD),[55] and LHb hyperactivation has been associated with both the neurobiological dysregulation and the motivational symptoms of depression.[56] We demonstrate a significant decrease in cAMP-stimulated PKA activity as well as altered dendritic localization of "active" free PKA catalytic subunits in MHb of the RIIαKO mouse. Given the direct and unidirectional input from the MHb to LHb,[17] it seems likely that input to the LHb is likely also impacted by the altered MHb PKA signaling in RIIαKO mice. Decreased LHb activity inversely impacts local DA activity that has downstream effects on VTA, a pathway that has notable overlap with the VTA-lateral hypothalamus-NAc pathway. Impaired DA signaling is a common thread that connects compulsive behaviors related to food intake, substance abuse and the motivation symptoms of depressive disorders. In both obesity and substance abuse, the dysregulation of DA signaling and subsequent changes in reward circuitry can fuel the cycle of compulsive drug or compulsive food consumption.

Altered DA signaling downstream of MHb after chronic HFD exposure was evidenced in the RIIαKO mouse by decreased striatal DARPP-32 T^{34} phosphorylation (Fig 3D). In intact neurons, T^{34} phosphorylation inhibits protein phosphatase 1, that in turn inhibits D_1 DA signaling.[42] After roux-en-Y gastric bypass, mice had increased DA D1R activity and reduced fat intake via PPARα-vagal-D1R signaling, unlike sham operated mice.[57] Additionally, studies in the ΔFos-overexpressing mouse, a model of increased reward sensitivity confirm the importance NAc feedback to the VTA in regulating DA signaling and moderating HFD intake. While chronic HFD led to decreased mRNA expression of tyrosine hydroxylase and DA transporter in VTA of control mice, levels of both were increased in the reward-sensitive ΔFos mouse.[43]

Blunted sucrose intake was a clear phenotypic characteristic of mice lacking *Prkar2a* and was strongest in males (Fig 4D-E). Whereas sucrose intake escalated in WT mice after its introduction and a high level of daily sucrose intake was maintained, the intake pattern for RIIαKO mice suggests decreased motivation and altered reward processing. It is important to note that RIIαKO mice prefer both HFD and sucrose solution when offered the choice between normal chow or HFD and 10% sucrose or water, respectively. The significant decrease in breakpoint, time engaged in the task, and number of rewards earned during operant progressive ratio tasks in fasted RIIαKO compared to WT mice further suggests the presence of an intact reward circuit, but decreased appetitive motivation that could lead to the "moderation" phenotype seen in RIIαKO mice with respect to palatable foods.

Sucrose preference and the behavioral and physiologic responses to chronic HFD exposure were sex-dependent in RIIαKO mice. Our observations with regards to sex differences in the recorded behaviors and metabolic parameters are consistent with other mouse models of PKA deficiency or overexpression, in which sexual dimorphism is a common characteristic.[58] While the requirement to include females in clinical and basic research protocols is relatively recent, mounting evidence suggests key differences in the regulation of behaviors linked to DA (and other monoamine) signaling. We report a more pronounced decrease in sucrose intake and preference in male compared to female RIIαKO mice, while decreases in intake, weight gain and metabolic efficiency during chronic HFD feeding were significant only in female KO mice. Clinical studies of depressive disorders reinforce key differences in the prevalence of depression and the response to anti-depressant drugs between sexes.[59] Binge-eating is more frequent in women,[36] a findings that is replicated in rodents.[37] Thus the inhibition of HFD intake in female mice via *Prkar2a* deletion is particularly interesting. Additionally, depression is more prevalent in females,[60] who are also significantly more sensitive to the anti-depressive effects of ketamine[61] and traditional SSRI anti-depression drugs via an ovarian hormone dependent mechanism.[61] In MDD, women

353 experience greater anxiety and somatic symptoms that include disturbances in sleep, appetite and
354 pain.[62] Sex-dependent mid-brain monoamine regulation likely underlies a number of signaling processes
355 involved in mood, intake of palatable foods and the pleasure derived from naturally rewarding
356 behaviors including those observed in the RIIαKO mouse. Further interrogation of behavior and
357 physiologic responses to both rewarding and aversive stimuli in male and female RIIαKO mice may
358 provide deeper insight into the mechanisms that underly the observed differences. Our data show that
359 comparable reductions in Hb PKA activity and neurotransmitter levels in Hb and IPN in male and female
360 mice elicit distinct effects in reward signals that can impact intake and body weight.

361

362 The dysregulated PKA signaling induced via *Prkar2a* deletion in the MHb causes decreased acetylcholine
363 release in both the Hb and the IPN, as well as decreased glutamate levels in the IPN (Figs 2B-C). Hb
364 acetylcholine signaling has been linked to both nicotine addiction and the aversive aspects of
365 withdrawal,[63] depressive disorders,[64] and more recently nicotine addiction has been linked to impaired
366 glucose control via Hb-gut connections.[4] While downregulation of cholinergic signaling caused
367 anhedonia-like behavior but not despair,[64] the developmental ablation of MHb neurons using a *Pou4f*-
368 cre driver in mice blunted both voluntary exercise and sucrose drinking, without other depression-
369 related symptoms.[8] Here we show that impaired *Prkar2a* regulation of PKA activity in MHb clearly
370 enhances the drive for voluntary exercise that could occur by altered localization of active PKA or
371 decreased total activity. However, the previously described mouse models and disease states such as
372 MDD and other depressive disorders, obesity, and in the first two of the three stages of the drug
373 addiction cycle (intake/binge, aversive cycles),[65] involve the regulation of these drives in the same
374 direction. *Prkar2a* is expressed in heterogenous cell populations within the dMHb and vMHb, in both
375 substance P- and acetylcholine-expressing cells and is expressed in glia and neurons which likely explains
376 the differential regulation of exercise and food reward drives. We have shown the direct impact of

Prkar2a deletion on acetylcholine and glutamate levels. *Prkar2a* is also highly expressed in *Tac1*- and *Tac2*-expressing cells of the MHb and thus, further study of PKA regulation in the various distinct cell subtypes is warranted.

Apart from what was learned from studies in the ΔFos-overexpression and *Pou4f*-cre driven MHb neuronal ablation mouse models, the RIIαKO mouse implicates the downregulation of PKA activity in MHb in the regulation of two overlapping but distinct pathways. Re-expression of Prkar2a in Hb of the global RIIαKO mouse rescued the sucrose and running phenotypes confirming that both behaviors are mediated by changes in habenular PKA signaling. Whereas the observed blunted response to sucrose and HFD and the decreased appetitive drive to obtain food rewards in the fasted state resemble anhedonia-like behaviors associated with MDD, the decreased locomotor typically observed with anhedonia is absent in this mouse model. While the connections to food reward behaviors in the RIIαKO mouse are clearer, the link to enhanced voluntary activity seems more complicated despite the known relationship between reward seeking and locomotor sensitization.[66] The inverse regulation of consummatory drive and the drive to engage in exercise caused by *Prkar2a* deficiency generates a desirable phenotype of sucrose and HFD intake moderation and of enhanced motivation for exercise. We identify habenular *Prkar2a* as a new player in regulating the habenular complex (aka, dorsal diencephalic conduction system), and provide new insights into the role of habenular PKA signaling, the regulation of hedonic drive and susceptibility to dietary obesity.

Methods

Mice. RIIαKO mice were obtained from MMRRC and have previously been described.[26] RIIα heterozygous breeding pairs were bred on a C57/Bl6 background to generate WT and KO littermates. This mouse line has been bred in our mouse facilities for approximately 10 years which ensures >99% C57/Bl6 background. A standard 0600h:1800h light/dark cycle was consistently maintained with an average temperature of 73°F. Mice were all handled regularly by the same individuals for the at least 2-3 weeks leading up the behavioral studies.

Ad libitum HFD feeding studies. To measure intake of palatable chow we used Bio-Serv #F3282, soft high-fat diet (HFD) that provides 5.49 kcal/g and derives approximately 15%, 59% and 26% of total energy from protein, fat and carbohydrate, respectively. Young adult (12–16-week old) male and female WT and RIIαKO littermates were individually housed and provided free access to drinking water and HFD. Body weight and weight of the food consumed were measured weekly for 3 weeks. Mice were maintained on the same 12h light:dark cycle and temperature and humidity conditions that they had been acclimated to from birth.

Sucrose intake and sucrose preference test. Sucrose preference was evaluated in individually housed WT and RIIαKO littermates by providing identical bottles containing water and 10% (w/v) sucrose solution side by side daily for three consecutive days a week for two weeks. The position of sucrose and water were alternated daily, and the amounts of sucrose solution and water consumed were determined by weighing each bottle when removed from the cage, and for sucrose solution, before replacement with

fresh solution. Absolute sucrose solution, water and control chow (CD) (NIH-31) intakes were analyzed, and sucrose preference was calculated as a percent (preference= sucrose solution intake (g) / (water intake (g) + sucrose solution intake (g)) *100.

Operant conditioning positive reinforcement studies. Young adult mice (3-6 months old) were individually housed in cages with a divider and calorie restricted for 1 week to achieve 90% of initial body weight and maintained on an 85% calorie restricted diet for the initial conditioning phase. Briefly, 85% of ad libitum intake was determined based on the average daily intake for 3 days. Once 90% of starting body weight was achieved, body weight was monitored daily and caloric restriction continued with adjustments made as needed to ensure optimal weight throughout the training phase. Purified Rodent Dustless Precision Pellets (14 mg, Bio-Serv) were used as food rewards.

Mice were randomly assigned to either right or left lever press and were trained with a fixed ratio 1 (FR1) schedule in which one food pellet was delivered for each correct lever press. The criteria for successful completion of the FR1 and FR5 tasks was receiving 50 food pellets with ≥80% correct lever presses within the 60-minute test period. Upon successful completion of the FR1 task for two consecutive days, mice progressed to the FR5 schedule and then to the progressive ratio (PR). Ad libitum feeding was reintroduced for FR5 and PR portions of the study.

Voluntary running behavior and blocked running wheel experiments. Individually housed young adult mice (3-6 months old) were provided with home cage running wheels for two weeks (Med Associates Inc, Fairfax VT). Daily running and total wheel turns were analyzed as 30-minute bins for the entire two-

week period. To test the effects of blocking the anticipated natural reward of running on immediate early gene (IEG) expression in habenula we used mice that had been provided free access to home cage running wheels for 2 weeks prior (n=4-6/group). Running wheels were locked but left inside of home cages 2h prior to the onset of the dark cycle (1600h). Between 1.5-2.5h post dark cycle onset, when running levels are typically high (1930-2030h), mice were transcardially perfused and brains harvested and processed as later described for immunofluorescent staining for c-Fos and c-Jun.

Dissection of brain for PKA enzymatic activity, ELISA, and western blot. Brains were cut into 150–200 µM thick sections and kept cold while dissected using a microscope (SMZ 1500, Nikon). Prefrontal cortex, striatum and habenula were dissected based on stereotaxic coordinates using the following landmarks: prefrontal cortex (bregma 3.0–-2.5 mm), bilateral samples taken just above and excluding the orbital area; striatum (bregma 1.5–- 0.2 mm), bilateral samples below and on the interior side of the genu of the corpus callosum and along the exterior edge of the lateral ventricle; habenula (bregma -1.0– -2.0 mm), bilateral samples taken directly adjacent to third ventricle just below the stria medullaris and above the paraventricular nucleus of the thalamus; interpeduncular nucleus (IPN) (bregma -3.35– -3.45 mm) was taken from either side of the midline just dorsal to the middle cerebellar peduncle and ventral to the ventral tegmental decussation, based on *The Mouse Brain in Stereotaxic Coordinates* (Franklin & Paxinos).[67] Dissected samples were immediately snap frozen in liquid nitrogen and stored at -80°C until assay.

PKA enzymatic activity assay. Tissues were homogenized in freshly prepared lysis buffer (10 mM Tris-HCl (pH 7.5), 1 mM EDTA, and 1 mM dithiothreitol with 0.5 mM PMSF and protease inhibitor cocktail I (1:100; EMD Biosciences, La Jolla CA). BCA assays were performed as per manufacturer's protocol to

463 determine the total protein concentrations of samples (Pierce). Samples were diluted to 1 µg/µL and 10
464 µL of total protein was used for each reaction. PKA enzymatic assays were performed by kemptide
465 assay, using 25 µM kemptide (Leu-Arg-Arg-Ala-Ser-Leu-Gly), as previously described with and without
466 cAMP (5 µM).[68] All reactions for basal and cAMP-stimulated (total) PKA activity were carried out in
467 duplicate. Additionally, activity values for replicate reactions that were incubated in the presence of PKI
468 (5 nM) were subtracted from activity values to account for non-specific kinase activity.

469

470 *Quantification of acetylcholine*. IPN acetylcholine concentrations were determined by
471 choline/acetylcholine assay kit (Abcam, cat# ab65345) as per manufacturers protocol. Samples were
472 weighed prior to homogenization to standardize the total amount of tissue analyzed. Tissues had been
473 previously snap frozen after micro-dissection from 150-200 µM thick sections at bregma -3.45– -3.5 mm
474 as previously described. After snap freezing, samples were stored at -80°C.

475

476 *Western blotting*. Habenular and striatal lysates were prepared as described for PKA enzymatic activity
477 assays. 10 µg of total protein per lane was loaded onto 4–12% Bis-Tris gels (Bolt Plus, Invitrogen) and
478 run for 35 min at 165 V. For each gel, 7 µL of WesternSure pre-stained protein ladder was loaded onto a
479 separate lane (Li-Cor).Protein was transferred onto nitrocellulose membranes using a semi-dry
480 apparatus for 30 min (TransBlot Turbo, BioRad), stained with Ponceau S stain, washed with 1X TBS with
481 0.1% Tween-20 (1X TBST) and then blocked with 5% nonfat dry milk or bovine serum albumin in 1X TBST
482 for 1 h at room temperature. Membranes were then probed overnight with primary antibodies with
483 gentle shaking at 4°C before washing 3 times with 1X TBST and probing for 1 h at room temperature
484 with the appropriate antibody and Precision Protein StrepTactin-HRP Conjugate (1:10,000, BioRad). All

485 western blots were visualized using either Pierce enzyme chemiluminescent substrate (Pierce) and a
486 ChemDoc analyzer (BioRad). See Supplemental Table 1 for antibodies used, sources and dilutions used.

487

488 *RNA extraction and relative mRNA expression analysis*. RNA was extracted from previously snap frozen
489 Hb that had been stored at -80°C. RNA was extracted by adding 500uL Trizol (Invitrogen) to each sample
490 in a microcentrifuge tube pre-loaded with RNAse free beads and homogenized using a Bead Ruptor Elite
491 (Omni International) for 2 X 20 seconds at a speed of 2.4. Samples were centrifuged for 5 minutes at
492 12,000 x g at 4°C. Supernatant was transferred to a clean tube for each sample and incubated for 5
493 minutes before adding 100 µL of chloroform, shaking by hand for 30 seconds and incubating for an
494 additional 3 minutes. Samples were centrifuged for 15 minutes at 12,000 x g at 4°C. The aqueous phase
495 was carefully removed and RNA quantified by nanodrop. 500 ng of total RNA was used to make cDNA
496 for each sample using SuperScript III First Strand Synthesis Supermix for qRT-PCR per manufacturer's
497 protocol (Invitrogen). Quantitative reverse transcriptase polymerase chain reaction (qRT-PCR) was
498 performed on a VIIA7 instrument (BioRad) using a standard 40 cycle program that included melt curve
499 analysis. To determine relative mRNA expression levels of PKA subunits in habenula, the following
500 specific, pre-optimized primers were used (*Prkar1a*: FW 5'-CGAAGAATCCTCATGGGAAG-3', REV 5'-
501 CTCTCCTTGCACCACGATCT-3' ; *Prkaca*: FW 5'-GAAAATCGTCTCTGGGAAGGT-3', REV 5'-
502 TGGCAATCCAGTCAGTCGT-3; *Rplp0: FW* 5'- GAAAATCTCCAGAGGCACCA-3', REV 5'-
503 ACCCTCCAGAAAGCGAGAGT-3'; *18S:* FW 5'-*GCAATTATTCCCCATGAACG*-3', REV 5'-
504 *GGCCTCACTAAACCATCCAA*-3'. Syber Green *Power* mastermix (10 uL), 1uL of cDNA, 8.4 uL H_2O and 0.3 uL
505 of each primer (10 µM) were combined for each reaction well and each reaction was performed in
506 triplicate (Applied Biosystems, VIIA7). Relative expression was determined using the $2^{-\Delta\Delta CT}$ values that
507 were calculated based on the average CT values for the housekeeper genes determined to be optimal

for the sample type (*18S* and *Rplp0*) and values were analyzed as the fold-change from WT values.[69] Melt curves and gel electrophoresis were used to confirm the expected pcr products.

Immunofluorescence. Mice were killed by slow replacement of air with CO_2 (flow rate ≤ 5L/min) followed by cervical dislocation. Mice were transcardially perfused with ice cold 1X PBS (10mL), followed by 4% paraformaldehyde (PFA) (20mL). Whole brains were post-fixed for 1h in 4% PFA, washed 3X with 1X PBS, then cryopreserved in 30% sucrose until brains sunk. Brains were washed again 3X with 1X PBS, and snap frozen in -80°C 2-methylbutane. Floating sections (35µM) were blocked with 5% donkey serum in 1X PBS with 0.1% Triton-X 100 and 0.1% glycine for 1h. Sections were incubated with primary antibodies overnight at 4°C with gentle shaking, then washed 3X with 1X PBS with 0.1% Triton-X 100 and then incubated with appropriate secondary antibodies for 1h at 4°C with gentle shaking. Sections were then washed 3X with 1X PBS with 0.1% Triton-X 100 and counterstained with DAPI (1:1000; Sigma Alrich). Antibodies were diluted in 2X diluted blocking buffer. See Supplementary Table 1 for antibodies and conditions used.

RNA in situ hybridization. Brains harvested from RIIαKO and WT littermates were immediately snap frozen in isopentane and stored at -80°C until cryo-sectioning. Brains were equilibrated at -20°C for at least 1h prior to sectioning (20 µM thick) on a cryostat (Leica) and mounted directly onto Superfrost slides (Fisher Scientific). Slides were sealed in an airtight bag and stored at -80°C and then fixed in ice cold 4% PFA for 1h at 4°C prior to use. After fixation, slides were dipped in ice-cold 1X PBS, and then dehydrated in an ethanol gradient from 50% to 100% for 5 minutes at each step. Slides were stored in fresh 100% ethanol for up to 7 days at -20°C prior to hybridization. *In situ* hybridization was performed by first pre-treating sections with a RNAScope protease inhibitor IV for 20 minutes and then probed

using specific probes (Suppl Table 2) and counterstained with DAPI following the manufacturer's protocol (RNAScope, ACD Bioscience).

Fluorescent microscopy. For *in situ* hybridization expression studies, immunofluorescence experiments and cellular localization studies, images were captured using a confocal microscope with fluorescent filters while maintaining uniform exposure settings across samples within each experimental batch (Zeiss LS800, Germany). A magnification of either 20X (for cell counting and *Prkar2a* colocalization with markers) or 63X with oil (dendrite localization) was used.

Quantification of colocalization of Prkar2a with MHb markers. Colocalization analyses were done using the Zen Blue software (Zeiss LS800, Germany). Sections were probed for *Prkar2a* and one to two other markers of MHb cell subtypes including *Tac1, Tac1R, Tac2, Slc17a7,* and *Chat*, and then counterstained with DAPI. Zen Blue software was used to perform the particle and density analyses (Zeiss, Germany). The polygon drawing tool was used to outline the MHb as the area of interest. The colocalization tool was used as per the manufacturer recommended procedure to determine colocalization between *Prkar2a* and another marker and is widely used for such quantifications (Everett, M. Acquiring and Analyzing Data for Colocalization Experiments in AIM or ZEN Software).[70] Colocalization thresholds were kept constant within each brain section. The utilized data point was the colocalization coefficient 1: Rhoda-T3, which describes the ratio of colocalized points for *Prkar2a* and the targeted marker to total *Prkar2a* points in the selected area.

c-Fos- and c-Jun-positive cell counting. c-Fos or c-Jun stained brain sections from mice that were either blocked from or permitted to continue running as previously described were imaged with a confocal microscope using uniform settings (Zeiss LS800) and analyzed using ImageJ software (NIH, Bethesda). The color channels for each image were split apart. Analyses were conducted solely on the red channel image. An outline of the MHb was created using the polygon drawing tool. Image threshold was set to allow for analysis of only legitimate signal. Threshold settings were kept uniform throughout the analysis of each sample. Amount of image particles was obtained using the 'Analyze Particles' function. Particle density ratio was calculated by the equation: (number of particles /area ratio of the MHb), the latter defined as the area of the MHb over the total image area. Area measurements were obtained using the 'Measure' function.

rAAV-mediated re-expression of Prkar2a. The construct, pAV-EF1a-mPrkar2a-IRES-eGFP, was generated and packaged into an adeno-associated virus (serotype AAV8) (titer: 1.44x10^13 GC/mL) (Vigene Bio, Rockville MD) (Figure 6). For construct validation, the vector was transfected into Hek293 cells (Transfectamine 2000, Invitrogen), and cells were lysed at 48h post-transfection to confirm expression of *Pkrar2a* and GFP gene products. Survival surgery was performed on male and female RIIαKO and WT mice (n=9-11/genotype) using aseptic techniques. Mice were anesthetized with 5% isoflurane and mounted on a stereotaxic frame with an integrated a computer atlas (Leica Angle Two) to aid with injection angles. Topical lidocaine/prilocaine cream (2.5%/2.5%) and buprenorphine (0.1 mg/kg via subcutaneous injection) were administered for post-operative analgesia. Following midline incision, 1 mm holes were drilled bilaterally at the following injection sites: anterior/posterior: -1.53 mm from bregma, lateral: (-/+) 0.17 mm, depth: -2.5 mm. A glass micropipette was used to deliver a volume of 100 nL of rAAV at a flow rate of 0.1 µL/min at 10.08° angles. Retrobeads (Lumafluor) were used initially to confirm the injection coordinates. Mice were provided with topical lidocaine/antibiotic ointment and

ketoprofen daily for at least 3 days following surgery and were observed regularly during the two-week recovery period that also enabled expression of the target proteins prior to behavior testing. Upon completion of post-rAAV injection behavior testing, mice were sacrificed and perfused, and brains prepared for immunofluorescence as described below. rAAV-injections were validated by fluorescent microscopy targeted to habenula and surrounding areas (Keyence, Japan) (Suppl Fig 2). RIIαKO and WT mice in which habenular expression of GFP and RIIα expression was not achieved were excluded from the experimental data.

Statistics. GraphPad Prism version 8.4.2 was used for all statistical analyses. Alpha was set at 0.05 and a *P* value of < 0.05 was considered as significant. When applicable, two-way unpaired t-test were used to compare WT and RIIαKO mouse data when normality assumptions were met. For data that were not normally distributed, the Mann Whitney rank test was used. For data sets including multiple time points, repeated measures two-way ANOVA analysis was used to evaluate the effect of genotype and of genotype and time on intake levels and preference. The Geisser-Greenhouse correction was used as needed to correct for unequal variability of differences. Multiple comparisons for one-way and two-way ANOVA analyses were done using Bonferroni's post hoc test to compare individual mean values for HFD intake, sucrose intake and preference between genotypes. Two-way unpaired t-tests were used for data that were normally distributed and the Mann-Whitney rank test were applied to data that did not meet the normality assumptions. Tests used and P value ranges are detailed in the figure legends.

Study approval. All procedures were carried out in accordance with the National Institute of Child Health and Human Development Animal Care and Use Committee guidelines.

599 Acknowledgements: Funding by the *Eunice Kennedy Shriver* National Institute of Child Health and
600 Human Development Division of Intramural Research. We would like to thank Daniel Abebe for his
601 invaluable help in setting up the murine behavior testing and Oksana Gavrilova for her guidance on
602 phenotyping and thought provoking discussions about experimental design.

603

604 Author contributions: Edra London designed and conducted the mouse behavioral studies, the
605 biochemical, histological, and molecular biology experiments and microscopy; managed data and data
606 analysis and statistics and prepared the manuscript. Jason Wester designed, optimized, and performed
607 all stereotaxic surgeries, provided guidance on data presentation and analyses, and contributed to the
608 manuscript preparation. Michelle Bloyd conducted the mouse behavioral studies, optimized
609 methodologies for analyzing the Prkar2a localization and IEG cell counting data, assisted with sample
610 preparation, and manuscript preparation. Shelby Bettencourt conducted the mouse behavioral studies
611 and assisted with the related data compilation and analyses, sample preparation and contributed to the
612 preparation of the manuscript. Chris McBain provided input regarding experimental design and data
613 analyses and contributed to manuscript preparation. Constantine Stratakis contributed to the project
614 and experimental design, data analyses and manuscript preparation.

1 Hikosaka, O. The habenula: from stress evasion to value-based decision-making. *Nat Rev Neurosci* **11**, 503-513, doi:10.1038/nrn2866 (2010).

2 Mathis, V. & Kenny, P. J. From controlled to compulsive drug-taking: The role of the habenula in addiction. *Neurosci Biobehav Rev* **106**, 102-111, doi:10.1016/j.neubiorev.2018.06.018 (2019).

3 Mathieu-Kia, A. M., Pages, C. & Besson, M. J. Inducibility of c-Fos protein in visuo-motor system and limbic structures after acute and repeated administration of nicotine in the rat. *Synapse* **29**, 343-354, doi:10.1002/(sici)1098-2396(199808)29:4<343::aid-syn6>3.0.co;2-5 (1998).

4 Duncan, A. *et al.* Habenular TCF7L2 links nicotine addiction to diabetes. *Nature* **574**, 372-377, doi:10.1038/s41586-019-1653-x (2019).

5 Antolin-Fontes, B. *et al.* The habenular G-protein-coupled receptor 151 regulates synaptic plasticity and nicotine intake. *Proc Natl Acad Sci U S A* **117**, 5502-5509, doi:10.1073/pnas.1916132117 (2020).

6 Matsumoto, M. & Hikosaka, O. Lateral habenula as a source of negative reward signals in dopamine neurons. *Nature* **447**, 1111-1115, doi:10.1038/nature05860 (2007).

7 Grigsby, K. B., Kelty, T. J. & Booth, F. W. Medial habenula maturational deficits associate with low motivation for voluntary physical activity. *Brain Res* **1698**, 187-194, doi:10.1016/j.brainres.2018.08.016 (2018).

8 Hsu, Y. W. *et al.* Role of the dorsal medial habenula in the regulation of voluntary activity, motor function, hedonic state, and primary reinforcement. *J Neurosci* **34**, 11366-11384, doi:10.1523/JNEUROSCI.1861-14.2014 (2014).

9 Viswanath, H., Carter, A. Q., Baldwin, P. R., Molfese, D. L. & Salas, R. The medial habenula: still neglected. *Front Hum Neurosci* **7**, 931, doi:10.3389/fnhum.2013.00931 (2013).

10 Cadd, G. & McKnight, G. S. Distinct patterns of cAMP-dependent protein kinase gene expression in mouse brain. *Neuron* **3**, 71-79, doi:10.1016/0896-6273(89)90116-5 (1989).

11 London, E. *et al.* Differentially regulated protein kinase A (PKA) activity in adipose tissue and liver is associated with resistance to diet-induced obesity and glucose intolerance in mice that lack PKA regulatory subunit type IIalpha. *Endocrinology* **155**, 3397-3408, doi:10.1210/en.2014-1122 (2014).

12 Lenard, N. R. & Berthoud, H. R. Central and peripheral regulation of food intake and physical activity: pathways and genes. *Obesity (Silver Spring)* **16 Suppl 3**, S11-22, doi:10.1038/oby.2008.511 (2008).

13 Boulos, L. J., Darcq, E. & Kieffer, B. L. Translating the Habenula-From Rodents to Humans. *Biol Psychiatry* **81**, 296-305, doi:10.1016/j.biopsych.2016.06.003 (2017).

14 Volkow, N. D., Wang, G. J., Fowler, J. S., Tomasi, D. & Baler, R. Food and drug reward: overlapping circuits in human obesity and addiction. *Curr Top Behav Neurosci* **11**, 1-24, doi:10.1007/7854_2011_169 (2012).

15 Geisler, S. & Trimble, M. The lateral habenula: no longer neglected. *CNS Spectr* **13**, 484-489, doi:10.1017/s1092852900016710 (2008).

16 Stamatakis, A. M. *et al.* Lateral Hypothalamic Area Glutamatergic Neurons and Their Projections to the Lateral Habenula Regulate Feeding and Reward. *J Neurosci* **36**, 302-311, doi:10.1523/JNEUROSCI.1202-15.2016 (2016).

17 Kim, U. & Chang, S. Y. Dendritic morphology, local circuitry, and intrinsic electrophysiology of neurons in the rat medial and lateral habenular nuclei of the epithalamus. *J Comp Neurol* **483**, 236-250, doi:10.1002/cne.20410 (2005).

18 Hsu, Y. W. *et al.* Medial habenula output circuit mediated by alpha5 nicotinic receptor-expressing GABAergic neurons in the interpeduncular nucleus. *J Neurosci* **33**, 18022-18035, doi:10.1523/JNEUROSCI.2927-13.2013 (2013).

19 Quina, L. A., Wang, S., Ng, L. & Turner, E. E. Brn3a and Nurr1 mediate a gene regulatory pathway for habenula development. *J Neurosci* **29**, 14309-14322, doi:10.1523/JNEUROSCI.2430-09.2009 (2009).
20 Contestabile, A. *et al.* Topography of cholinergic and substance P pathways in the habenulo-interpeduncular system of the rat. An immunocytochemical and microchemical approach. *Neuroscience* **21**, 253-270, doi:10.1016/0306-4522(87)90337-x (1987).
21 Lecourtier, L. & Kelly, P. H. A conductor hidden in the orchestra? Role of the habenular complex in monoamine transmission and cognition. *Neurosci Biobehav Rev* **31**, 658-672, doi:10.1016/j.neubiorev.2007.01.004 (2007).
22 Ren, J. *et al.* Habenula "cholinergic" neurons co-release glutamate and acetylcholine and activate postsynaptic neurons via distinct transmission modes. *Neuron* **69**, 445-452, doi:10.1016/j.neuron.2010.12.038 (2011).
23 Authement, M. E. *et al.* A role for corticotropin-releasing factor signaling in the lateral habenula and its modulation by early-life stress. *Sci Signal* **11**, doi:10.1126/scisignal.aan6480 (2018).
24 Biran, J., Palevitch, O., Ben-Dor, S. & Levavi-Sivan, B. Neurokinin Bs and neurokinin B receptors in zebrafish-potential role in controlling fish reproduction. *Proc Natl Acad Sci U S A* **109**, 10269-10274, doi:10.1073/pnas.1119165109 (2012).
25 Hu, F., Ren, J., Zhang, J. E., Zhong, W. & Luo, M. Natriuretic peptides block synaptic transmission by activating phosphodiesterase 2A and reducing presynaptic PKA activity. *Proc Natl Acad Sci U S A* **109**, 17681-17686, doi:10.1073/pnas.1209185109 (2012).
26 Burton, K. A. *et al.* Type II regulatory subunits are not required for the anchoring-dependent modulation of Ca2+ channel activity by cAMP-dependent protein kinase. *Proc Natl Acad Sci U S A* **94**, 11067-11072, doi:10.1073/pnas.94.20.11067 (1997).
27 Geisler, S., Derst, C., Veh, R. W. & Zahm, D. S. Glutamatergic afferents of the ventral tegmental area in the rat. *J Neurosci* **27**, 5730-5743, doi:10.1523/JNEUROSCI.0012-07.2007 (2007).
28 Aizawa, H., Kobayashi, M., Tanaka, S., Fukai, T. & Okamoto, H. Molecular characterization of the subnuclei in rat habenula. *J Comp Neurol* **520**, 4051-4066, doi:10.1002/cne.23167 (2012).
29 Wallace, M. L. *et al.* Anatomical and single-cell transcriptional profiling of the murine habenular complex. *Elife* **9**, doi:10.7554/eLife.51271 (2020).
30 Amieux, P. S. *et al.* Compensatory regulation of RIalpha protein levels in protein kinase A mutant mice. *J Biol Chem* **272**, 3993-3998, doi:10.1074/jbc.272.7.3993 (1997).
31 Yang, L., Gilbert, M. L., Zheng, R. & McKnight, G. S. Selective expression of a dominant-negative type Ialpha PKA regulatory subunit in striatal medium spiny neurons impairs gene expression and leads to reduced feeding and locomotor activity. *J Neurosci* **34**, 4896-4904, doi:10.1523/JNEUROSCI.3460-13.2014 (2014).
32 Sutherland, R. J. The dorsal diencephalic conduction system: a review of the anatomy and functions of the habenular complex. *Neurosci Biobehav Rev* **6**, 1-13, doi:10.1016/0149-7634(82)90003-3 (1982).
33 Hikosaka, O., Sesack, S. R., Lecourtier, L. & Shepard, P. D. Habenula: crossroad between the basal ganglia and the limbic system. *J Neurosci* **28**, 11825-11829, doi:10.1523/JNEUROSCI.3463-08.2008 (2008).
34 Bischoff, S. *et al.* Spatial distribution of GABA(B)R1 receptor mRNA and binding sites in the rat brain. *J Comp Neurol* **412**, 1-16 (1999).
35 Charles, K. J. *et al.* Comparative immunohistochemical localisation of GABA(B1a), GABA(B1b) and GABA(B2) subunits in rat brain, spinal cord and dorsal root ganglion. *Neuroscience* **106**, 447-467, doi:10.1016/s0306-4522(01)00296-2 (2001).

36 Hudson, J. I., Hiripi, E., Pope, H. G., Jr. & Kessler, R. C. The prevalence and correlates of eating disorders in the National Comorbidity Survey Replication. *Biol Psychiatry* **61**, 348-358, doi:10.1016/j.biopsych.2006.03.040 (2007).

37 Klump, K. L., Racine, S., Hildebrandt, B. & Sisk, C. L. Sex differences in binge eating patterns in male and female adult rats. *Int J Eat Disord* **46**, 729-736, doi:10.1002/eat.22139 (2013).

38 Wise, R. A., Spindler, J. & Legault, L. Major attenuation of food reward with performance-sparing doses of pimozide in the rat. *Can J Psychol* **32**, 77-85, doi:10.1037/h0081678 (1978).

39 Wise, R. A. Dopamine, learning and motivation. *Nat Rev Neurosci* **5**, 483-494, doi:10.1038/nrn1406 (2004).

40 Geiger, B. M. *et al.* Deficits of mesolimbic dopamine neurotransmission in rat dietary obesity. *Neuroscience* **159**, 1193-1199, doi:10.1016/j.neuroscience.2009.02.007 (2009).

41 Sharma, S. & Fulton, S. Diet-induced obesity promotes depressive-like behaviour that is associated with neural adaptations in brain reward circuitry. *Int J Obes (Lond)* **37**, 382-389, doi:10.1038/ijo.2012.48 (2013).

42 Svenningsson, P. *et al.* DARPP-32: an integrator of neurotransmission. *Annu Rev Pharmacol Toxicol* **44**, 269-296, doi:10.1146/annurev.pharmtox.44.101802.121415 (2004).

43 Teegarden, S. L., Nestler, E. J. & Bale, T. L. Delta FosB-mediated alterations in dopamine signaling are normalized by a palatable high-fat diet. *Biol Psychiatry* **64**, 941-950, doi:10.1016/j.biopsych.2008.06.007 (2008).

44 Rada, P., Bocarsly, M. E., Barson, J. R., Hoebel, B. G. & Leibowitz, S. F. Reduced accumbens dopamine in Sprague-Dawley rats prone to overeating a fat-rich diet. *Physiol Behav* **101**, 394-400, doi:10.1016/j.physbeh.2010.07.005 (2010).

45 Svenningsson, P. *et al.* Involvement of striatal and extrastriatal DARPP-32 in biochemical and behavioral effects of fluoxetine (Prozac). *Proc Natl Acad Sci U S A* **99**, 3182-3187, doi:10.1073/pnas.052712799 (2002).

46 Liu, M. Y. *et al.* Sucrose preference test for measurement of stress-induced anhedonia in mice. *Nat Protoc* **13**, 1686-1698, doi:10.1038/s41596-018-0011-z (2018).

47 Nieh, E. H. *et al.* Decoding neural circuits that control compulsive sucrose seeking. *Cell* **160**, 528-541, doi:10.1016/j.cell.2015.01.003 (2015).

48 Grant, J. Tachykinins stimulate a subset of mouse taste cells. *PLoS One* **7**, e31697, doi:10.1371/journal.pone.0031697 (2012).

49 Yoo, J. H. *et al.* Ventral tegmental area glutamate neurons co-release GABA and promote positive reinforcement. *Nat Commun* **7**, 13697, doi:10.1038/ncomms13697 (2016).

50 Paul, M. J., Indic, P. & Schwartz, W. J. A role for the habenula in the regulation of locomotor activity cycles. *Eur J Neurosci* **34**, 478-488, doi:10.1111/j.1460-9568.2011.07762.x (2011).

51 Rhodes, J. S., Garland, T., Jr. & Gammie, S. C. Patterns of brain activity associated with variation in voluntary wheel-running behavior. *Behav Neurosci* **117**, 1243-1256, doi:10.1037/0735-7044.117.6.1243 (2003).

52 Febbraro, F., Svenningsen, K., Tran, T. P. & Wiborg, O. Neuronal substrates underlying stress resilience and susceptibility in rats. *PLoS One* **12**, e0179434, doi:10.1371/journal.pone.0179434 (2017).

53 Cullinan, W. E., Herman, J. P., Battaglia, D. F., Akil, H. & Watson, S. J. Pattern and time course of immediate early gene expression in rat brain following acute stress. *Neuroscience* **64**, 477-505, doi:10.1016/0306-4522(94)00355-9 (1995).

54 Matsumoto, M. & Hikosaka, O. Representation of negative motivational value in the primate lateral habenula. *Nat Neurosci* **12**, 77-84, doi:10.1038/nn.2233 (2009).

55 Szczypinski, J. J. & Gola, M. Dopamine dysregulation hypothesis: the common basis for motivational anhedonia in major depressive disorder and schizophrenia? *Rev Neurosci* **29**, 727-744, doi:10.1515/revneuro-2017-0091 (2018).
56 Sartorius, A. & Henn, F. A. Deep brain stimulation of the lateral habenula in treatment resistant major depression. *Med Hypotheses* **69**, 1305-1308, doi:10.1016/j.mehy.2007.03.021 (2007).
57 Hankir, M. K. *et al.* Gastric Bypass Surgery Recruits a Gut PPAR-alpha-Striatal D1R Pathway to Reduce Fat Appetite in Obese Rats. *Cell Metab* **25**, 335-344, doi:10.1016/j.cmet.2016.12.006 (2017).
58 London, E., Bloyd, M. & Stratakis, C. A. PKA functions in metabolism and resistance to obesity: lessons from mouse and human studies. *J Endocrinol* **246**, R51-R64, doi:10.1530/JOE-20-0035 (2020).
59 Carrier, N. & Kabbaj, M. Sex differences in the antidepressant-like effects of ketamine. *Neuropharmacology* **70**, 27-34, doi:10.1016/j.neuropharm.2012.12.009 (2013).
60 Kessler, R. C. Epidemiology of women and depression. *J Affect Disord* **74**, 5-13, doi:10.1016/s0165-0327(02)00426-3 (2003).
61 Keers, R. & Aitchison, K. J. Gender differences in antidepressant drug response. *Int Rev Psychiatry* **22**, 485-500, doi:10.3109/09540261.2010.496448 (2010).
62 Carmona, N. E. *et al.* Sex differences in the mediators of functional disability in Major Depressive Disorder. *J Psychiatr Res* **96**, 108-114, doi:10.1016/j.jpsychires.2017.09.025 (2018).
63 Antolin-Fontes, B., Ables, J. L., Gorlich, A. & Ibanez-Tallon, I. The habenulo-interpeduncular pathway in nicotine aversion and withdrawal. *Neuropharmacology* **96**, 213-222, doi:10.1016/j.neuropharm.2014.11.019 (2015).
64 Han, S. *et al.* Down-regulation of cholinergic signaling in the habenula induces anhedonia-like behavior. *Sci Rep* **7**, 900, doi:10.1038/s41598-017-01088-6 (2017).
65 Volkow, N. D., Koob, G. F. & McLellan, A. T. Neurobiologic Advances from the Brain Disease Model of Addiction. *N Engl J Med* **374**, 363-371, doi:10.1056/NEJMra1511480 (2016).
66 Robinson, T. E. & Berridge, K. C. The neural basis of drug craving: an incentive-sensitization theory of addiction. *Brain Res Brain Res Rev* **18**, 247-291, doi:10.1016/0165-0173(93)90013-p (1993).
67 Paxinos, G., Franklin, K. B. J. & Franklin, K. B. J. *The mouse brain in stereotaxic coordinates*. 2nd edn, (Academic Press, 2001).
68 Nesterova, M., Yokozaki, H., McDuffie, E. & Cho-Chung, Y. S. Overexpression of RII beta regulatory subunit of protein kinase A in human colon carcinoma cell induces growth arrest and phenotypic changes that are abolished by site-directed mutation of RII beta. *Eur J Biochem* **235**, 486-494, doi:10.1111/j.1432-1033.1996.00486.x (1996).
69 Livak, K. J. & Schmittgen, T. D. Analysis of relative gene expression data using real-time quantitative PCR and the 2(-Delta Delta C(T)) Method. *Methods* **25**, 402-408, doi:10.1006/meth.2001.1262 (2001).
70 Everett, M. Acquiring and Analyzing Data for Colocalization Experiments in AIM or ZEN Software. (2011).

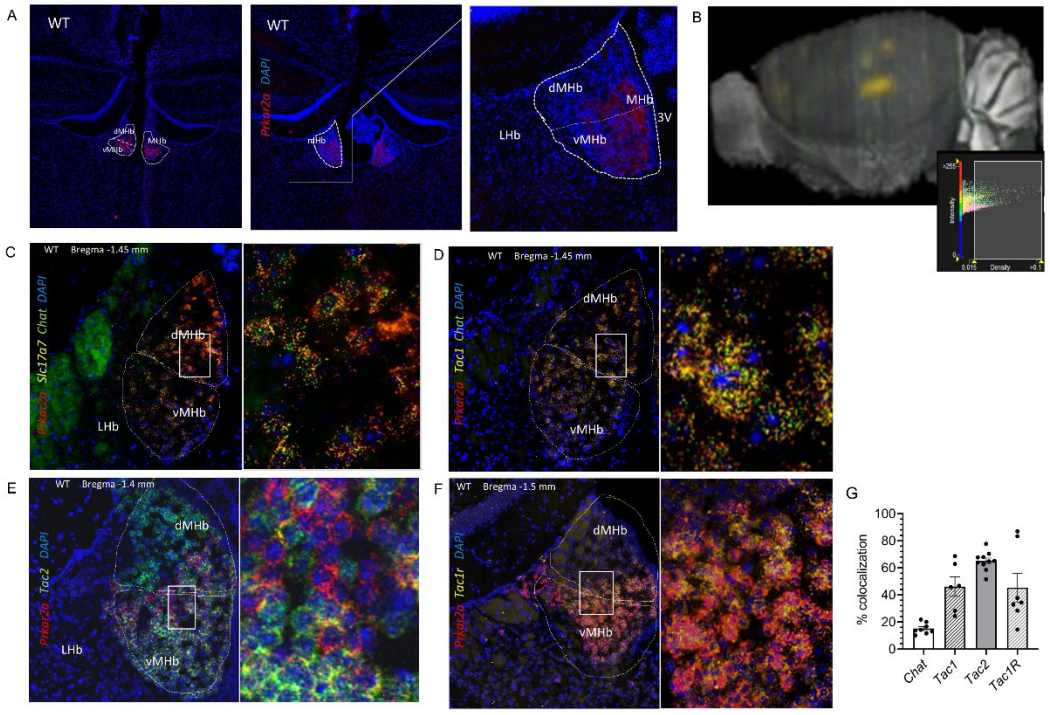

795

796 **Figure 1.** In brain, *Prkar2a* expression is nearly exclusive to habenula. A. *In situ* hybridization (ISH) for
797 *Prkar2a* (left) and immunofluorescence (IF) for PKA RIIα protein (right) with higher magnification detail
798 show that expression in WT (C57/Bl6) mouse brain is primarily in the MHb, and B. 3-D ISH for *Prkar2a*
799 shows robust and specific habenular localization of *Prkar2a* (3-D image: Allen Brain Institute).
800 Representative ISH images (and higher magnification details) show colocalization of *Prkar2a* with C.
801 *Slc17a7* and *Chat*, D. *Tac1* and *Chat*, E. *Tac2* and F. *Tac1r* in dMHb and VMHb. G. In MHb, *Chat*, *Tac1*,
802 *Tac2* and *Tac1R* were expressed in approximately 15%, 46%, 65%, and 40% of *Prkar2a* expressing cells;
803 n=6-11 sections from 3 different mice (1 male, 2 female) for each target; two-tailed unpaired t-tests; *,
804 $p < 0.05$. All data represent the mean ± sem.

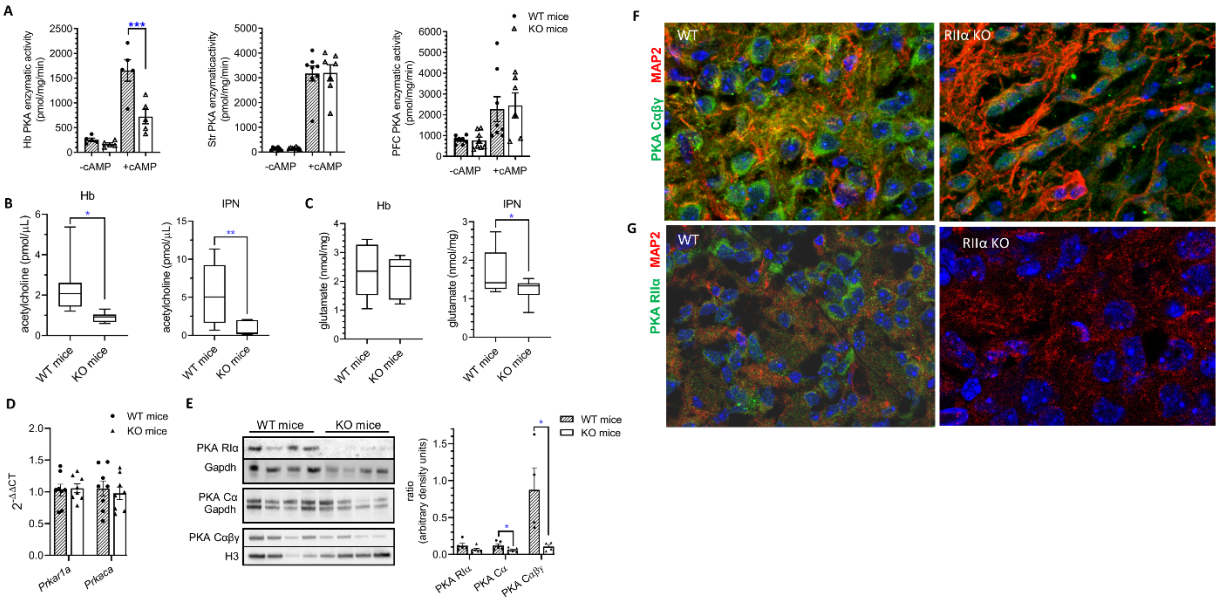

805

806 **Figure 2.** RIIαKO mice had reduced habenular PKA enzymatic activity, decreased interpeduncular
807 nucleus (IPN) acetylcholine and glutamate levels and altered localization of PKA catalytic subunit to
808 dendrites compared to WT mice. A. Basal and total (cAMP-stimulated) PKA enzymatic activities in Hb,
809 striatum (Stri) and prefrontal cortex (PFC); n=5-8/group (female data shown); ***, *P* <0.0001, unpaired
810 two-tailed t-tests, B. Acetylcholine concentrations in Hb and IPN were lower in RIIαKO mice compared to
811 WT littermates; n=6-7/sex/group (male data shown); **, p<0.01, unpaired two-tailed t-test. C.
812 Glutamate concentrations did not differ in Hb but were lower in IPN of KO compared to WT mice; n=7-
813 9/group (female (Hb) and male data (IPN) shown), *, p<0.05, unpaired two-tailed t-test, D. Habenular
814 *Prkar1a* and *Prkaca* mRNA levels did not differ between WT and RIIαKO mice; n=7/group (male data
815 shown), unpaired two-tailed t-tests, D. Representative western blots of Hb lysates for PKA subunits RIα
816 and Cα (first membrane with Gapdh as housekeeper, females) and combined Cαβγ (second membrane
817 with Histone 3 as housekeeper, males); n=4/genotype; unpaired two-tailed t-tests, *, p<0.05.
818 Representative immunofluorescent images of WT (left) and RIIαKO (right) brain sections (MHb) showed
819 differences in the subcellular localization of: E. PKA catalytic subunits (αβγ, green) in lower dMHb in WT,

820 and mutant mice that had impaired dendritic localization (shown by staining for MAP2, red), and F. PKA
821 RIIα (green) that is localized both to the cell body and dendrites (MAP2, red) in WT mice (female data
822 shown). All data represent the mean ± sem.

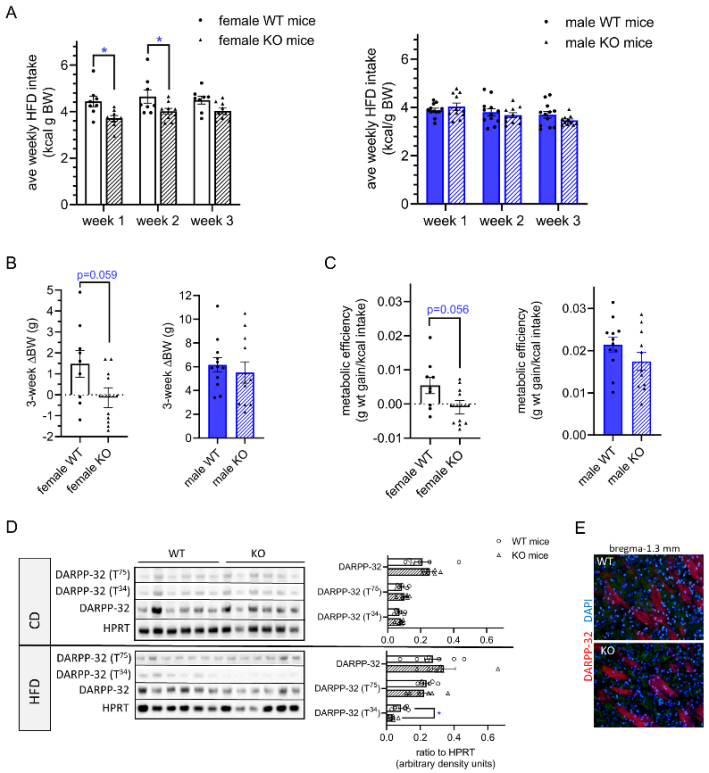

823

824 **Figure 3.** RIIαKO mice had decreased HFD intake, sucrose solution intake and sucrose preference
825 compared to WT mice and differences were influenced by sex. A. Average weekly intake of HFD during a
826 3-week period of *ad libitum* access was adjusted for body weight; n= 8–12/sex/genotype; repeated
827 measure two-way ANOVA with multiple comparisons (Bonferroni post hoc test). B. Difference in BW
828 (ΔBW) from outset of HFD intake experiment until the end of wk3 (1 negative data point for MKO not
829 shown on graph); n= 8–12/sex/genotype; two-way unpaired t-test; n= 8–12/sex/genotype, and C.
830 metabolic efficiency (kcal intake/wt gain) for female and male RIIαKO and WT mice during 3wk HFD-
831 feeding period (1 negative data point for FKO not shown on graph); n=9-12/sex/group, two-way
832 unpaired t-test. D. Representative western blot of striatal lysates from mice fed CD (top) or HFD (3wk)
833 (bottom) for DARPP-32 and DARPP-32 (T^{34}) with HPRT as the loading control and densitometry analysis;
834 two-way unpaired t-test, female data shown; E. Representative IF image of post-HFD (3wk) striatum
835 probed for DARPP-32 and counterstained with DAPI (n=3 mice/genotype, females).

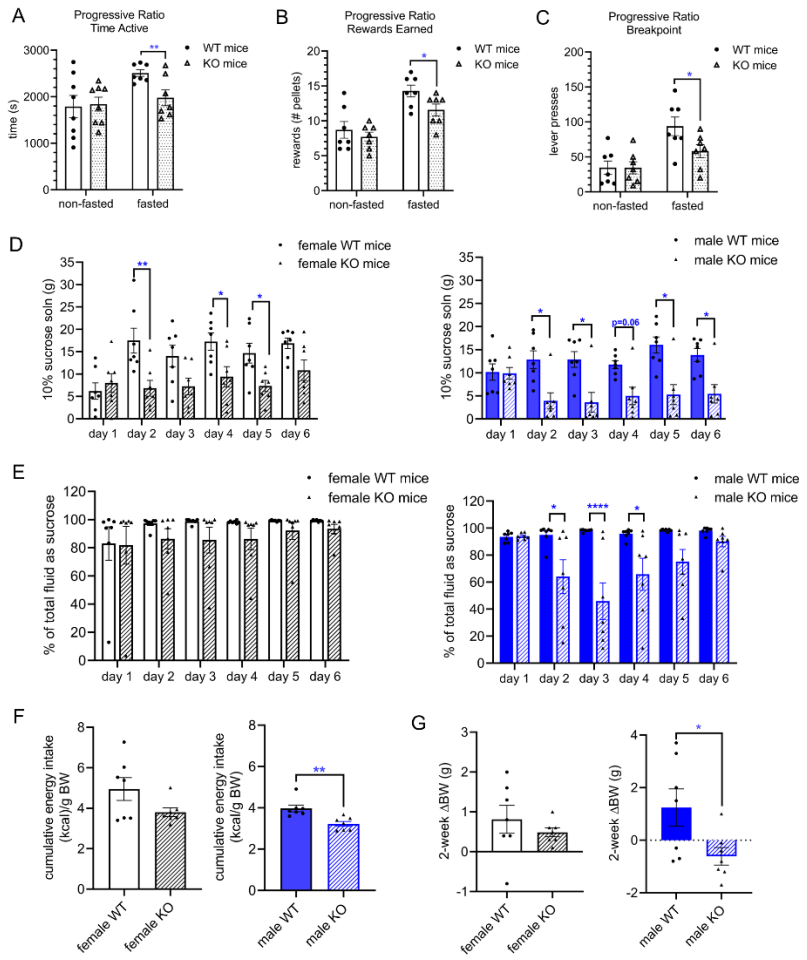

836

837 Figure 4. RIIαKO mice had decreased motivation for food rewards, decreased sucrose solution intake
838 and sucrose preference compared to WT mice; differences were influenced by sex. A. Amount of time
839 spent engaged in a progressive ratio operant task, B. breakpoint, and C. number of food pellets earned
840 by WT and RIIαKO littermates during progressive ratio operant task in fed and fasted states, n= 7-
841 8/group, (female mice), analyzed by unpaired two-way t-tests. D. Average daily intake of 10% sucrose
842 solution of female and male RIIαKO and WT mice; repeated measure two-way ANOVA with multiple
843 comparisons (Bonferroni post hoc test); and E. sucrose preference ((daily sucrose solution intake
844 (g)/total fluid intake (g)) X 100); sucrose intake and preference analyzed by repeated measure two-way
845 ANOVA with multiple comparisons (Bonferroni post hoc test). F. Cumulative total energy intake adjusted
846 for body weight for female and male mice during 2wk experiment, ((sucrose kcal + chow kcal)/ g BW),

analyzed by two-way unpaired t-test (male) and Mann Whitney non-parametric rank test (female), and G. Change in body weight during the 2wk sucrose intake experiment, analyzed by two-way unpaired t-test (male) and Mann Whitney (female). For sucrose studies, n=9-12/sex/group. All data are mean ± sem; *, $P < 0.05$; **, $P < 0.01$, ****, $P < 0.0001$.

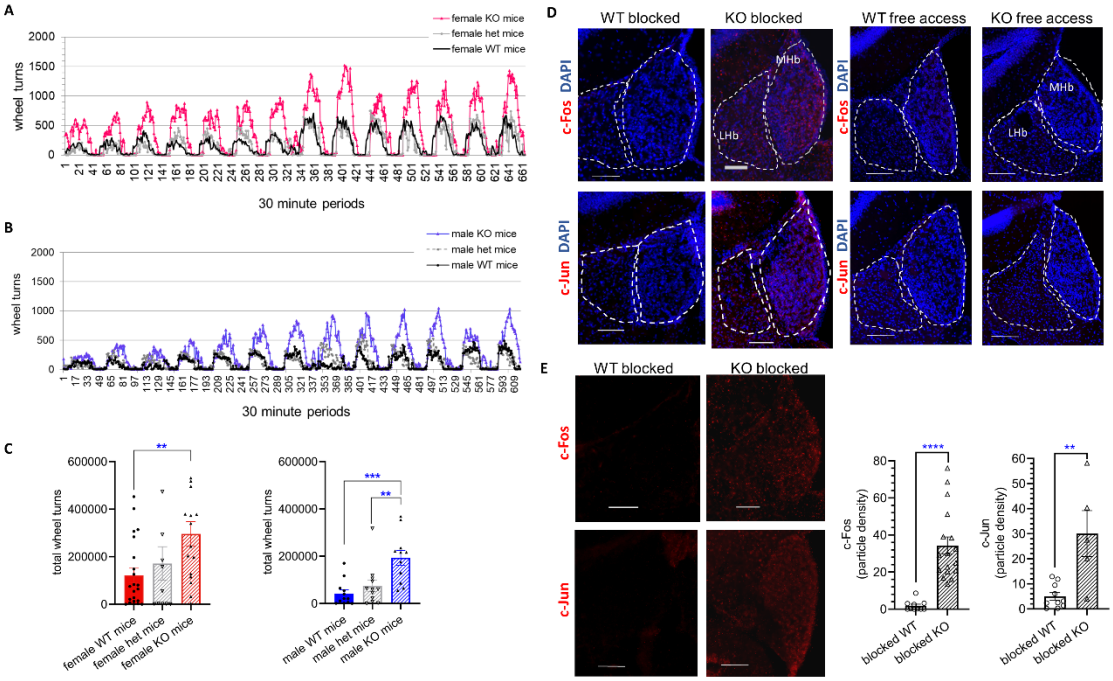

852

853 **Figure 5.** RIIαKO mice run more than twice the distance as their WT littermates during home cage
854 running wheel access. Heterozygosity for *Prkar2a* rescued the running phenotype. Voluntary running
855 activity was graphed in bins of 30 minutes over a two-week period for A. female (n=11-24/genotype),
856 and B. male (n=8-12/genotype) RIIαKO, RIIα+/- and WT mice, and C. the total number of wheel turns
857 during the 2wk period, analyzed by one-way ANOVA with multiple comparisons (Bonferroni's post hoc
858 test). D. Representative staining for c-Fos or c-Jun (red) (merged with DAPI) in WT and RIIαKO mice
859 either permitted to run as already acclimated for 2wk prior or blocked from running at the outset of the
860 dark cycle (1800h). E. The same images (4D) are shown with only c-Fos or c-Jun (red) and particle density
861 of c-Fos and c-Jun was analyzed with ImageJ software; unpaired two-way t-tests, n=5-17 sections from a
862 total 3-5 mice per IEG/genotype (3 males, 7 females). Particle density is defined as the number of
863 counted particles divided by the area ratio of the MHb, with the latter being the area of the MHb over
864 the total image area. All data represent mean ± sem; scale bars represent 100 µM; *, $P < 0.05$; **, $P <$
865 0.01, ***, $P < 0.001$, ****, $P < 0.0001$.

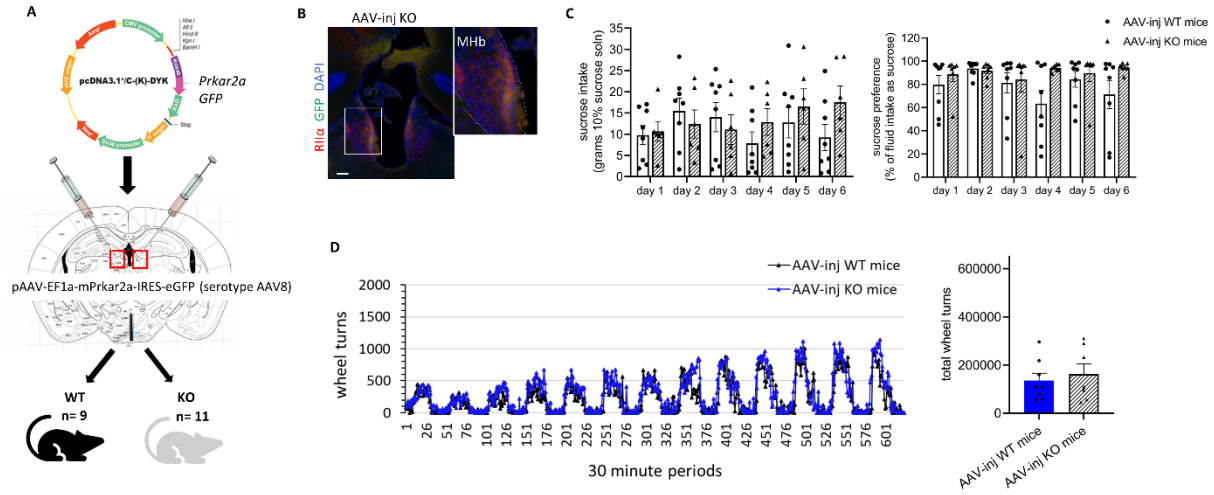

866

867 **Figure 6.** Stereotaxic rAAV-mediated re-expression of *Prkar2a* rescued the sucrose and running
868 phenotypes of RIIαKO mice. A. Map of *Prkar2a* expression vector used to generate injectable rAAV and
869 diagram of the injection strategy, B. Representative image of coronal section from injected RIIAKO
870 mouse of a successful rAAV-inection with expression of RIIα and GFP in MHb with magnified portion on
871 right; scale bar represents 100 µM, C. Sucrose intake and sucrose preference tests for rAAV-injected WT
872 and KO mice revealed no differences between genotypes (n=6-8/group; 7 males, 7 females), and D. 2wk
873 running wheel activity of rAAV-injected WT and KO mice did not differ between genotypes; (n=7-
874 8/group; 6 males, 9 females), repeated measure two-way ANOVA with multiple comparisons
875 (Bonferroni's post hoc test) and a two-tailed t-test were used for sucrose and running analyses,
876 respectively; all data represent the mean ± sem.